Research Report

Experimental Study on Opening Delay of a Reed Valve for Compressors: Visualization of Oil Film Behaviors and Measurement of Valve Deformations in the Opening Process

Fumitaka Yoshizumi, Kazunori Yoshida, Takahiro Moroi, Shinji Tamano and Yohei Morinishi

Report received on Oct. 25, 2012

ABSTRACT Automatic reed valves are widely used to control refrigerant gas flow in reciprocating compressors for automotive air conditioners. The oil film in the clearance between the reed and the valve seat causes a delay in the opening of the valve. This opening delay of the discharge valve leads to over compression, which increases losses such as friction in sliding components and gas overheating. Therefore, it is important to understand the valve behavior both in terms of the oil film and the elastic reed deformation in order to reduce losses due to the delay.

This study aims to develop an experimental setup that enables simultaneous visualization of oil film rupture and measurement of reed deformation and to observe this behavior during the valve opening process. The oil film rupture is visually observed using a high-speed camera through a special valve seat made of glass. The total deformation of the cantilever reed is identified by multipoint strain measurement with 12 strain gauges.

The results indicate that the opening process is divided into four stages. In the first stage, the reed remains stuck to the seat and deforms as the bore pressure increases. In the second stage, cavitation occurs in the oil film, and the film starts to rupture. In the third stage, the oil film ruptures, and the bore pressure starts to decrease. Finally, in the fourth stage, the reed is separated from the seat, and the gas flows through the valve. Reducing the reed/seat contact area changes the reed deformation in the first stage, thereby increasing the reed/seat distance and realizing an earlier oil film rupture and a shorter delay.

KEYWORDS Compressor, Valve, Flow Visualization, Elastic Deformation, Oil Film, Cavitation

1. Intoroduction

Recently, higher air-conditioner efficiency has become an important issue with regard to improvement of vehicle fuel economy. Energy loss in an automotive air conditioner mainly occurs in the compressor. The reciprocating-type compressor shown in **Fig. 1** is widely used in automotive air conditioners. The efficiency of this type of compressor is greatly influenced by the suction and discharge performance of the refrigerant gas at the reed valves. In particular, reducing the energy loss caused by the discharge valves is important.

A typical discharge reed valve is shown in **Fig. 2**. The reed valve consists of a reed (a thin plate) and a valve seat. The valve opens and closes automatically depending on the pressure difference between the inside and the outside of the cylinder bore. The energy loss of the discharge process is mainly caused by over compression of the refrigerant gas. Over compression leads to larger mechanical losses due to friction in the sliding components and larger refrigeration cycle losses due to gas overheating. Over compression is caused by the opening delay of the discharge valve and the refrigerant flow loss. This study focuses on the opening delay.

The opening delay of the reed valve is considered to be caused by the inertia of the reed and the negative squeeze effect (the squeeze effect of liquid films

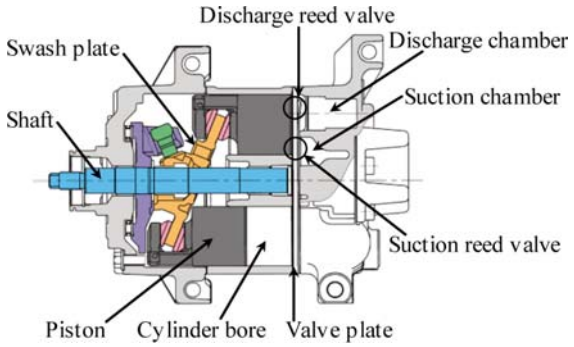

Fig. 1 Reciprocating compressor (Positive displacement type).

between two surfaces under separating) of the refrigerant oil that exists between the reed and the valve seat. This oil is included in the refrigerant to lubricate the moving parts. The negative squeeze effect of the oil is estimated to be the principal cause of the opening delay. In previous studies, parameters such as the oil viscosity, reed thickness, and reed/seat contact area have been investigated experimentally[1-6] and theoretically[1,7-12] to determine the relationships between these parameters and the delay. However, the detailed dynamic behavior of the reed opening, including the interaction of the reed deformation and the negative squeeze effect of the oil film, has not yet been identified.

With the goal of improving the valve opening delay, we have experimentally analyzed the transient reed elastic deformation that occurs in accordance with the oil film behavior.[13,14] An experimental setup was developed to simultaneously measure the strain distribution of the reed and observe the oil film rupture. Through this setup, the interaction of the reed deformation and the oil film behavior in the valve opening delay was investigated by changing the seat configuration. The results are summarized in this paper.

2. Nomenclature

g gravitational acceleration
P_b bore pressure
P_{b0} initial bore pressure
P_o discharge pressure
H thickness of the reed
t time
x, y, z Cartesian coordinates
δ bending displacement of the reed (displacement in the z direction)
δ_{gs} δ measured by the gap sensor located at the center of the port
ε strain
θ bending slope of the reed
κ curvature of the reed

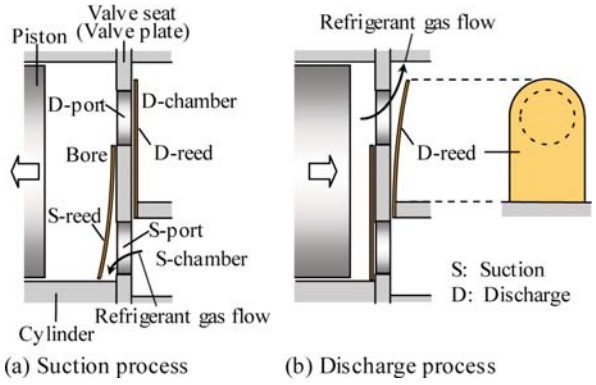

Fig. 2 Mechanism of reed valve in suction and discharge processes.

3. Experimental

3. 1 Experimental Setup

The overall system setup is shown in **Fig. 3**. The setup simulates the discharge valve opening process using compressed air. The setup consists of a pneumatic circuit system and a measurement system.

The pneumatic circuit system contains two pressure sources. One is a low-pressure source that simulates pressures below the discharge pressure, and the other is a high-pressure source that simulates pressures above the discharge pressure. These two pressure sources are connected to the test section through a three-port electromagnetic valve.

The details of the test section are shown in **Fig. 4**. The valve seat is made of glass, and a steel reed is mounted on it and clamped at the root end to create a cantilever support. The thickness H of the reed is 0.38 mm. The bore walls are made of acrylic acid resin. These transparent seat and bore walls enable the oil film between the reed and the seat to be observed visually.

This measurement system simultaneously measures the oil film behavior, the bore pressure, the reed displacement, and the reed strain. The oil film between the reed and the seat was observed by a high-speed camera (NAC, ST-709) through the seat and bore chamber. The bore pressure was measured by a pressure transducer (KULITE, XT-140-500A, accuracy: ±0.0035 MPa) attached to the end of the pipe (ϕ1 mm) connected to the bore. The reed displacement at the center of the port was measured by a gap sensor (eddy current sensor, AEC PU-05, ϕ5 mm, resolution: 0.3 μm). The strain distribution on the reed surface was measured by 12 wire strain gauges (KYOWA, KFG-1-120-D9-11, KFG-1-120-D16, KFR-02N-120-C1-11) affixed to the discharge side (the lengths of the gauges were 1 mm, except for (11) and (12), which were 0.2 mm). A two-axis gauge (rosette gauge) was affixed

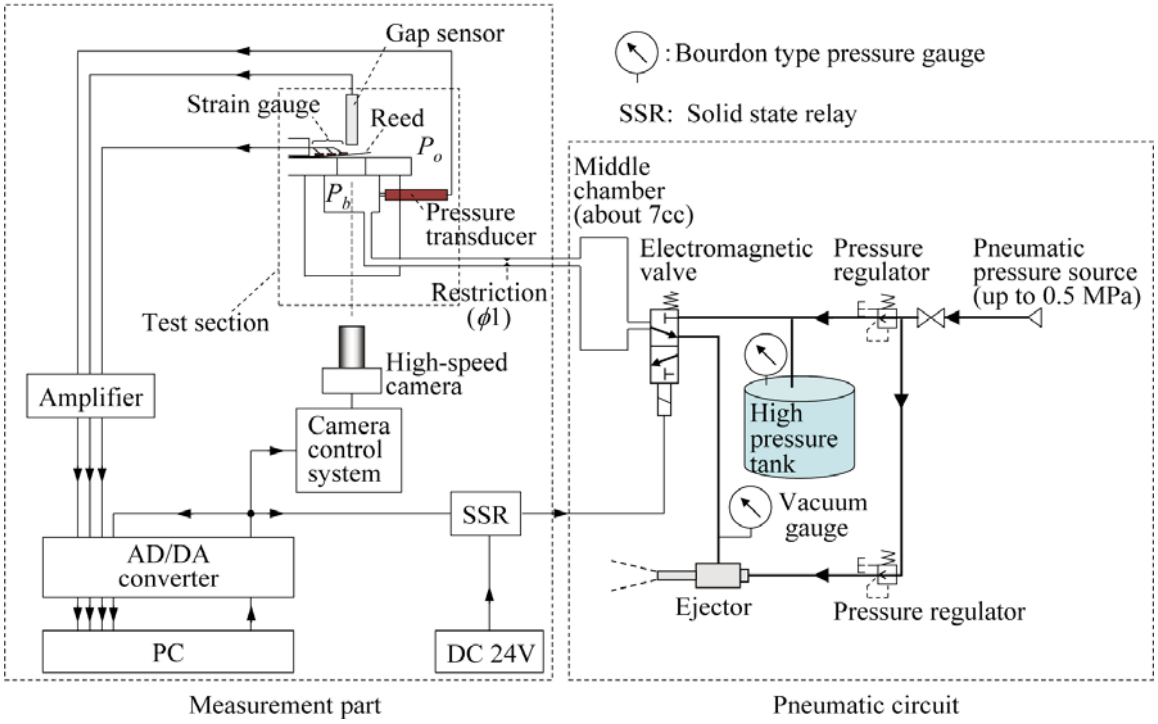

Fig. 3 Experimental setup.

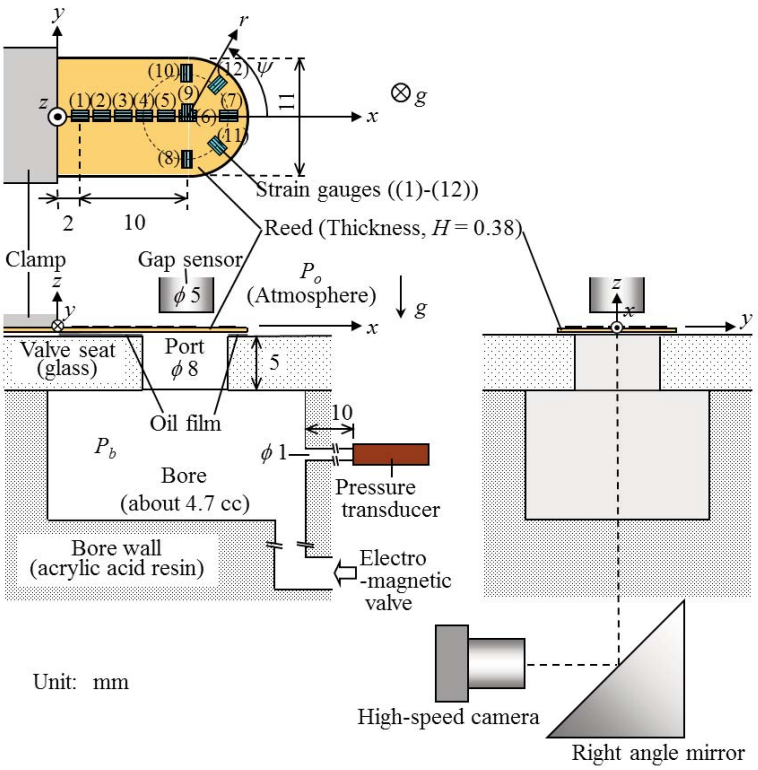

Fig. 4 Details of test section

to the center of the port. The strain distribution in the longitudinal direction of the reed (x direction) was measured by gauges (1)-(7), covering the region from the support position (called the "root" below) to the free tip end. The strain in the radial direction around the port was measured by gauges (4), (7), (8), (10), (11), and (12). Between the cases with and without gauges, there was no significant difference in the maximum bore pressure over the uncertainty in the experiment. The pressure values in this report are written as absolute pressure values (not as gauge pressure values).

3. 2 Measuring Procedure and Conditions

Before testing, the pressure of the high-pressure source was regulated to determine the initial rate of change in the bore pressure (dP_b/dt). The refrigerant oil (polyalkylene glycol-based synthetic, viscosity: 9×10^{-2} Pa·s, density: 9.9×10^2 kg/m^3) was injected into the gap between the reed and the seat using a hypodermic syringe. The amount of oil injected before each test was 0.1 cc, which is sufficient to fill the gap across the entire contact area. After injecting the oil, a pressure below atmospheric pressure was applied to the bore by the low-pressure source, and the test was started. A common trigger signal from a personal computer (PC) was used to control the switching of the electromagnetic valve and the recording of the high-speed camera and other sensor signals, as shown in **Fig. 5**. The trigger signal from the PC was also recorded to synchronize the camera images and other sensor signals.

The discharge pressure was set to atmospheric pressure (P_o = 0.101 MPa, 20.5°C ± 1.5°C). The pressure of the low-pressure source, i.e., the initial bore pressure P_{b0}, was regulated to 0.087 MPa. The pressure of the high-pressure source was regulated to 0.32 MPa, and the averaged rate of change of the bore pressure in the 0.01 s period after $P_b = P_o$ was dP_b/dt = 7.8 MPa/s. The sampling frequency of the sensor signals was 20 kHz, and the frame rate of the high-speed camera was 10 000 fps.

The configurations of the two tested valve seats are shown in **Fig. 6**. The effect of the contact area between the reed and the seat was examined using two representative types of seats: SEAT A (without a groove around the port) and SEAT B (with a groove around the port). A common reed was used for both types of seats.

3. 3 Identification of Reed Deformation

The bending displacement (the displacement in the z direction) was estimated from the measured strain distribution. First, the bending displacement was calculated along the longitudinal direction (x direction) under the assumption that the bending mode can be expressed by the Euler-Bernoulli beam theory. The procedure is summarized as follows:

(1) The strain at the root (x = 0 mm) was assumed to be equal to the strain at the nearest gauge (gauge (1) in Fig. 4), and the strain at the free tip end (x = 17.5 mm) was set to zero.

(2) The curvature κ was calculated from the strain by $\kappa = \varepsilon/(H/2)$.

(3) The bending slope θ was obtained from the trapezoidal integral of the curvature with respect to x (**Fig. 7**). The bending displacement δ was obtained from the trapezoidal integral of the slope with respect to x. The root was assumed to be fixed (θ = 0 rad and δ = 0 mm at x = 0 mm). The slope and the displacement were determined sequentially from the root to the free tip end. The details of the calculation procedure are shown in Ref. (13).

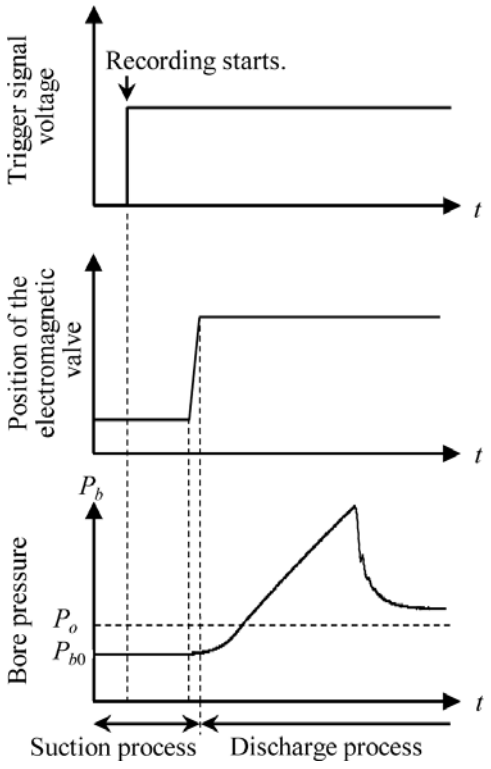

Fig. 5 Trigger signal and bore pressure.

Next, the bending displacement was also calculated along the width direction (y direction) using the trapezoidal integral of the strain. The strain at the edge was set to zero. The slope at the center ($y = 0$ mm) was assumed to be zero, and the displacement at the center was identical to that obtained in the procedure for the x direction. The slope and the displacement were determined sequentially from $y = 0$ mm.

4. Results and Discussion

4. 1 Outline of Opening Process

First, the entire opening process was observed through the reed displacement at the port center δ_{gs} and the bore pressure P_b. Time series diagrams for P_b and δ_{gs} of both the SEAT A and SEAT B are shown in **Fig. 8**. The time origin ($t = 0$ ms) corresponds to the moment that the bore pressure reaches the discharge pressure ($P_b = P_o$), which is the ideal time for the valve to begin to open. The displacement and the deformation of the reed can be defined as the variation from the position at $t = 0$ ms.

For both seat types, the opening process is divided into four stages. Although the period of each stage depends on the type of seat, i.e., the contact area, both types show the same phenomenon in each stage. In the stiction stage (Stage I), the reed continues to stick to the seat as the bore pressure increases. Reed deformation takes place with increasing bore pressure. In the pre-rupture stage (Stage II), the reed starts to leave the seat as the bore pressure keeps increasing. In the rupture stage (Stage III), reed displacement rapidly increases, and the bore pressure starts to decrease. In the full-open stage (Stage IV), the reed is separated completely from the seat over the entire area of the cantilever, and the gas flow settles down to a steady state.

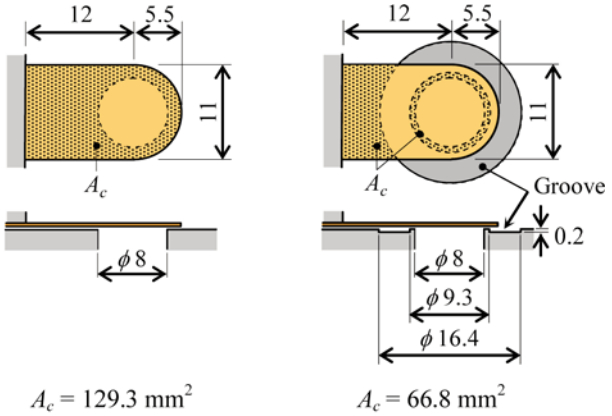

Fig. 6 Geometry of reed valves.

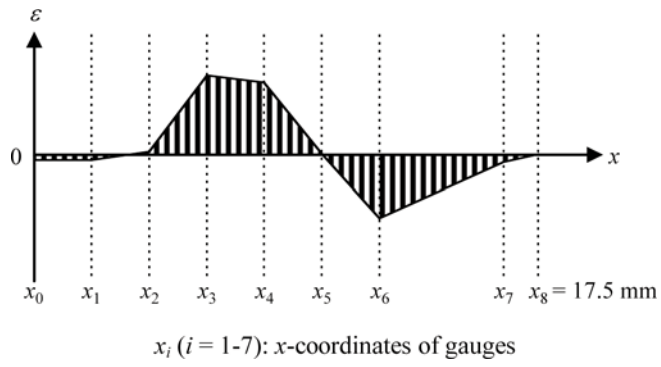

Fig. 7 Trapezoidal integral for strain profile.

4. 2 Observation in Each Stage

For the SEAT A, the time history of the reed deformation and the oil film behavior were observed in each stage. **Figure 9** shows the reed deformation in the x-axis and y-axis directions during the stiction stage (Stage I). The oil film behavior around the port during the pre-rupture stage (Stage II) is shown in **Fig. 10**. **Figure 11** shows the process of the oil film rupture in the rupture stage (Stage III). A schematic of the oil film behavior is shown in **Fig. 12**. The change in the reed deformation along the x-axis during the pre-rupture and rupture stages (Stage II and Stage III) is shown in **Fig. 13**. The figures (except Fig. 10) are for the test shown in Fig. 8. The zoomed images in Fig. 10 were captured in another test with the same conditions.

4. 2. 1 Stiction Stage (Stage I)

In this stage, though the sequential images captured by the camera show no change (see Fig. 10(a) and Fig. 11(a)), reed deformation is observed. The bending deformation along the x-axis occurs intensively in the region of 4 mm $\leq x \leq$ 8 mm, and the reed leaves the seat slightly in the region of $x \geq 8$ mm, while the reed sticks to the seat in the region of $0 \leq x \leq 4$ mm. This means that the reed sticks to the seat at the root side area, and the actual fixed end is positioned in the region of 4 mm $\leq x \leq$ 8 mm. The reed also has a slight

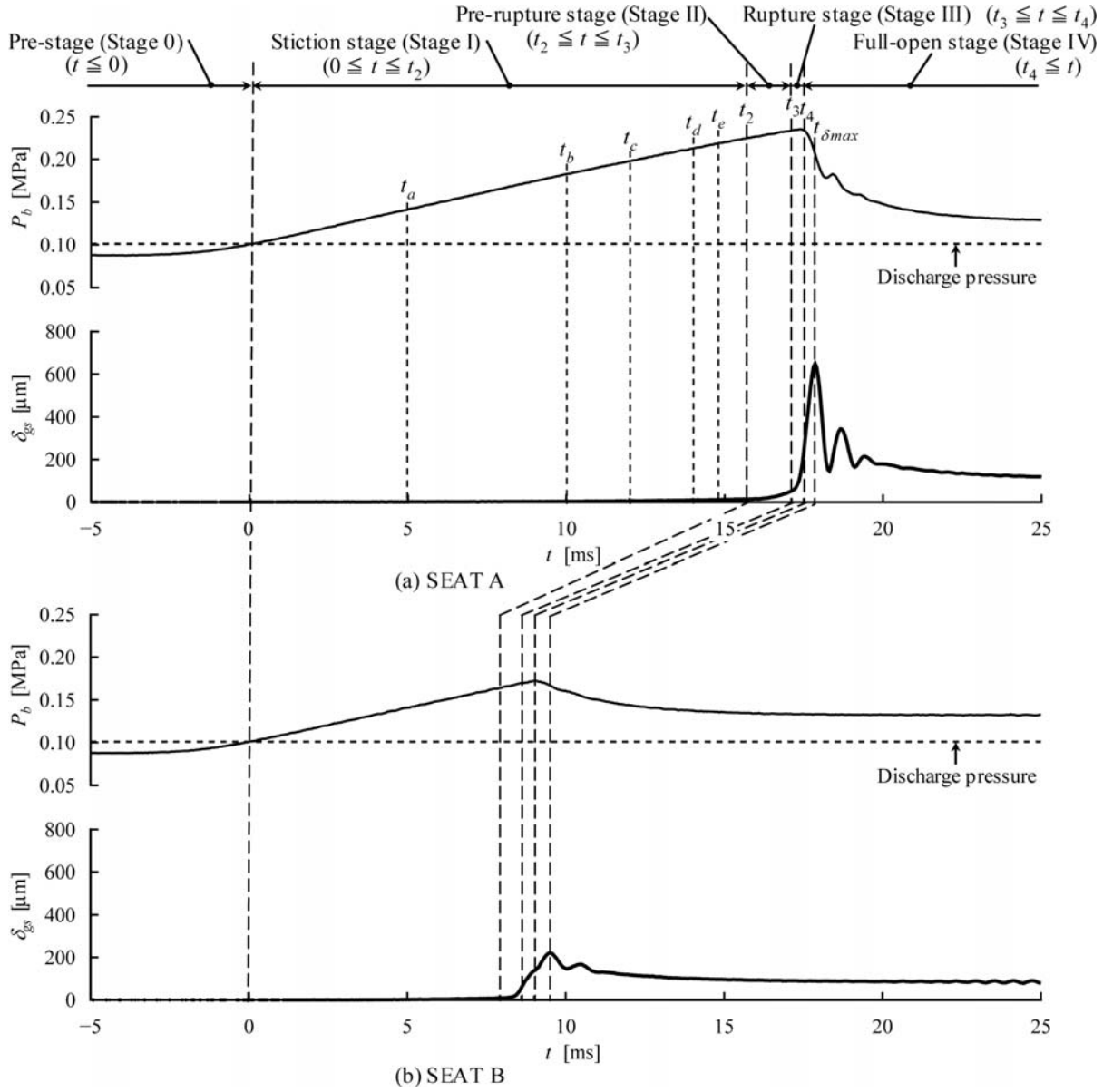

Fig. 8 Time series of reed displacement and bore pressure.

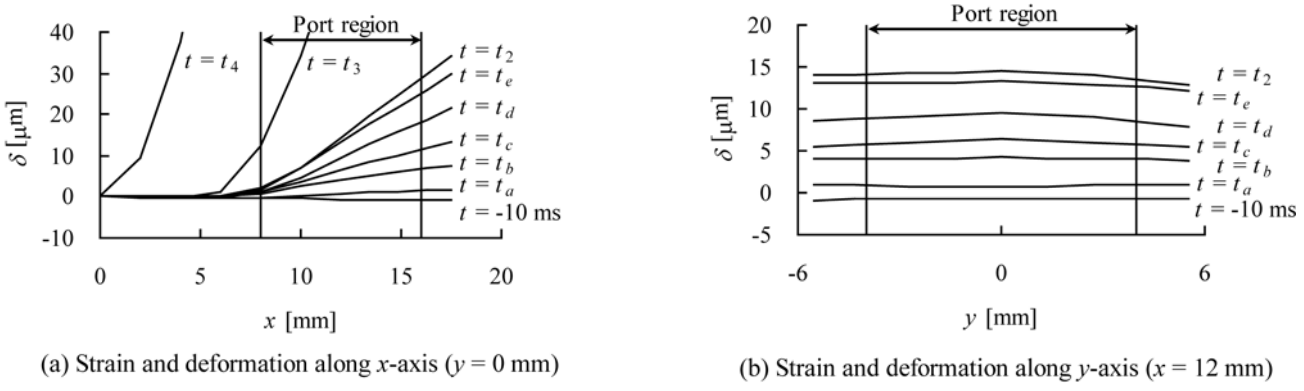

(a) Strain and deformation along x-axis (y = 0 mm)

(b) Strain and deformation along y-axis (x = 12 mm)

Fig. 9 Reed strain and deformation before oil film rupture. (SEAT A in Stage I of the test shown in Fig. 8.)

convex deformation towards the discharge side at the port and its surrounding area both along the *x*-axis (Fig. 9(a)) and the *y*-axis (Fig. 9(b)). The reed deformation consists of a bending deformation as a beam along the *x*-axis and a convex deformation as a shell on the port.

The convex deformation towards the discharge side and the stiction at the root side indicate that the oil film pressure becomes lower than the discharge pressure by the negative squeeze effect. The oil pressure and the reed deformation cause forces in the $-z$ direction, and the bore pressure causes a force in the $+z$ direction. The

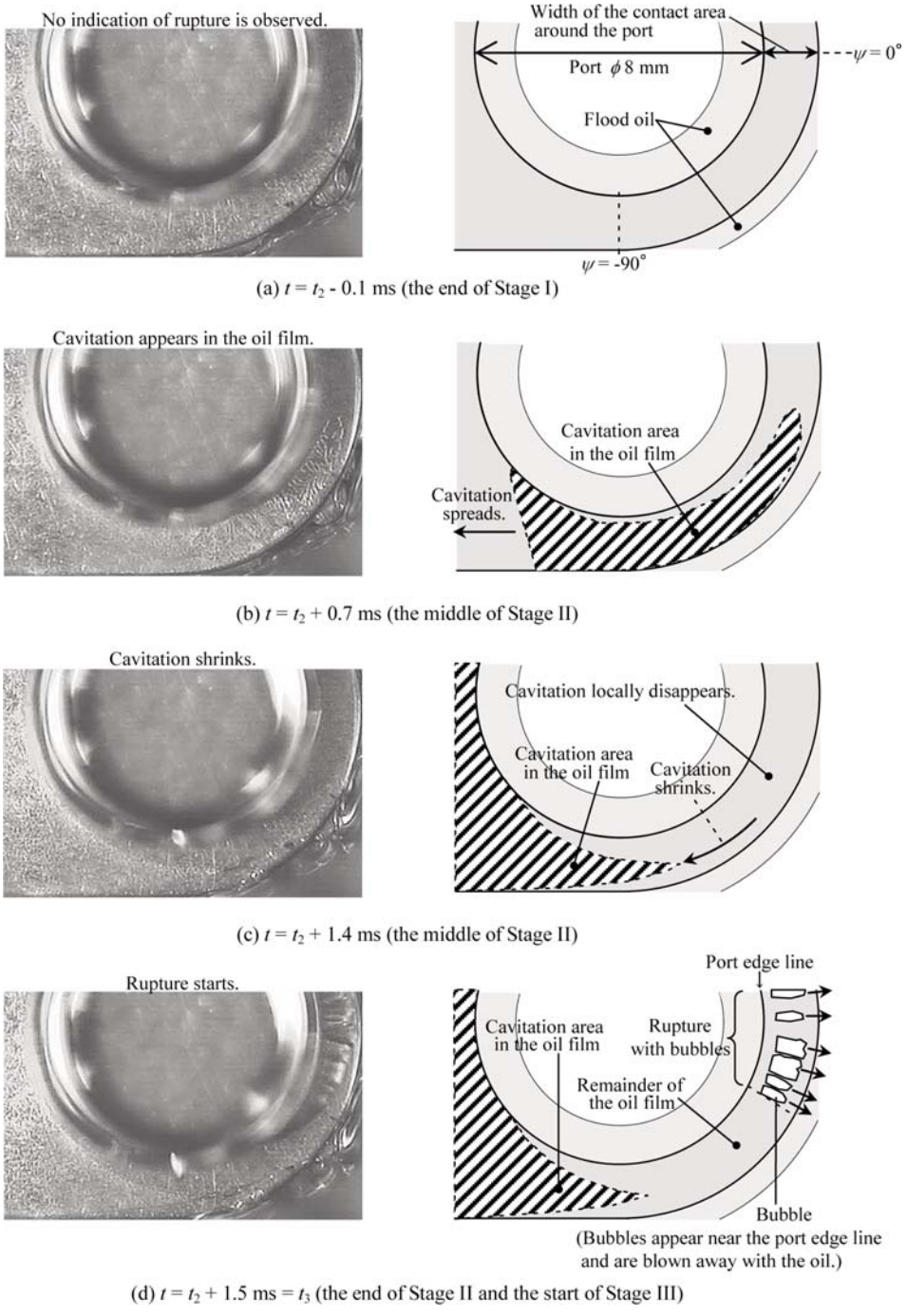

Fig. 10 Oil film images just before rupture. (SEAT A in Stage II; the images were captured in a test different from that of Fig. 8.)

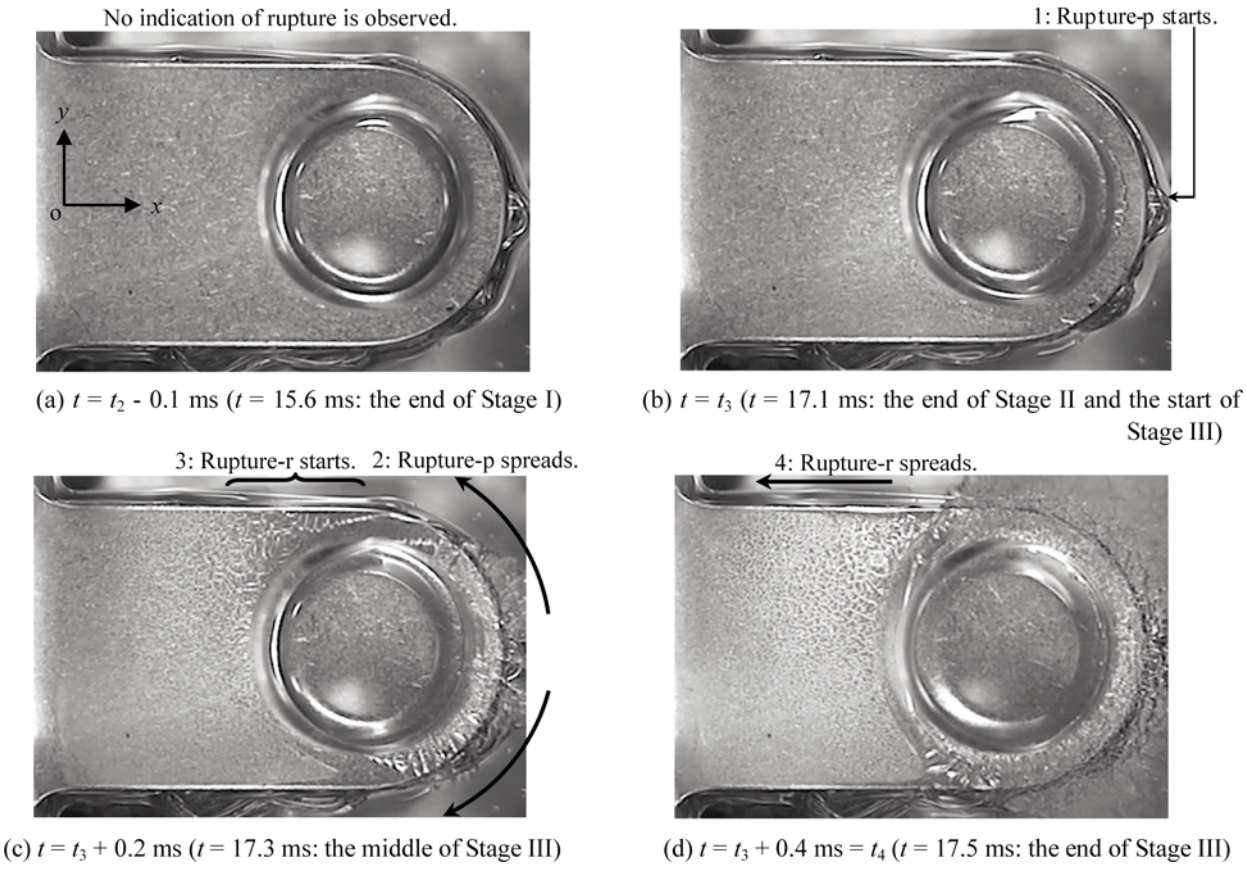

(a) $t = t_2$ - 0.1 ms (t = 15.6 ms: the end of Stage I)

(b) $t = t_3$ (t = 17.1 ms: the end of Stage II and the start of Stage III)

(c) $t = t_3 + 0.2$ ms (t = 17.3 ms: the middle of Stage III)

(d) $t = t_3 + 0.4$ ms = t_4 (t = 17.5 ms: the end of Stage III)

Fig. 11 Process of oil film rupture. (SEAT A in Stage II and Stage III; the images were captured in the test shown in Fig. 8; Rupture-p: Oil film rupture around the port, Rupture-r: Oil film rupture at the root area.)

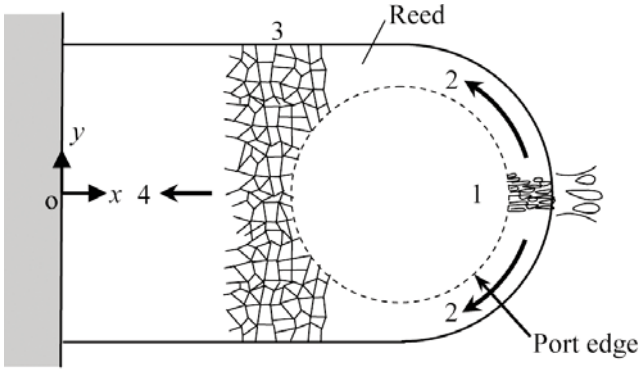

1: Rupture-p starts, $t = t_3$
2: Rupture-p spreads, $t_3 < t \leq t_3 + 0.6$ ms
3: Rupture-r starts, $t = t_3 + 0.2$ ms
4: Rupture-r spreads, $t_3 + 0.2$ ms $< t \leq t_3 + 0.4$ ms

Fig. 12 Illustration of oil film rupture (SEAT A in Stage III).

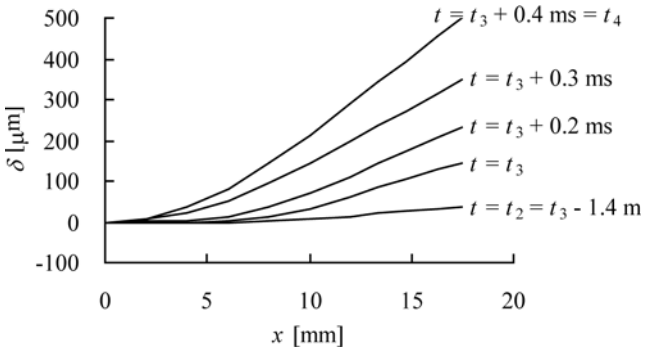

Fig. 13 Reed strain and deformation during oil film rupture. (SEAT A in Stage II and Stage III of the test shown in Fig. 8.)

inertial force of the reed is negligible (the order is 10^{-3} N, while the force from the bore pressure is 6.2 N at the end of Stage I), and the three above-mentioned forces maintain a quasi-static balance in Stage I.

4. 2. 2 Pre-rupture Stage (Stage II)

In this stage, cavitation occurs in the oil film at the seal area around the port, and rupture of the oil film starts. The oil film behavior in this stage is observed in the zoomed images shown in Fig. 10. No change is observed in the sequential images in Stage I (see Fig. 10(a)). In Stage II, first, the cavitation pattern starts to appear at a location near the free tip end, and this indicates that the stage changes to Stage II (see Fig. 10(b)). The pattern becomes clear and forms one cavity region with a boundary. Second, the cavitation pattern shrinks and disappears at the tip-side semicircle around the port, while the pattern spreads at the root-side semicircle around the port (see Fig. 10(c)). Finally, bubbles appear near the port edge line, and rupture of the oil film starts from the free tip end (see Fig. 10(d)). A previous study[4] proposed a model for the oil film taking the onset of cavitation into account. The visual observation in the present study supports the idea that cavitation occurs locally just before the oil film rupture.

4. 2. 3 Rupture Stage (Stage III)

In this stage, the rupture of the oil film spreads over the contact area (see Fig. 11(b), (c), and (d)). This stage consists of two processes: a process in which the rupture spreads around the port and a process in which the rupture spreads over the root-side area. In the former process, first, the oil film at the seal area around the port is locally blown away with bubbles in the outward radial direction (see "1: Rupture-p starts" in Figs. 11 and 12), and this indicates that the stage changes to Stage III. Second, the blowout of the oil spreads throughout the seal area around the port along the circumference (see "2: Rupture-p spreads" in Figs. 11 and 12). Simultaneously, the reed leaves the seat sequentially from the tip end to the port area (see $t = t_3$ + 0.2 ms in Fig. 13).

In the latter process, the cavitation pattern becomes clear at the root-side contact area near the port (see "3: Rupture-r starts" in Figs. 11 and 12). The cavitation pattern spreads towards the root of the cantilever (see "4: Rupture-r spreads" in Figs. 11 and 12). The reed leaves the seat sequentially from the port area to the root in accordance with the spreading cavitation pattern (see $t = t_3$ + 0.2 ms, $t = t_3$ + 0.3 ms, and $t = t_3$ + 0.4 ms in Fig. 13). The bore pressure reaches its maximum (0.235 MPa) and starts to decrease during the latter process ("4: Rupture-r spreads").

4. 2. 4 Full-open Stage (Stage IV)

The reed displacement reaches its maximum (648 μm) and experiences transient vibration, settling down to steady displacement (100 μm). The bore pressure also settles down to a steady value (0.127 MPa).

In order to capture the oil film image, the initial rate of the bore pressure in the present experiment is set to a low level of dP_b/dt = 7.8 MPa/s, which corresponds to a rotation speed of 100 rpm in real compressors, while the usual rotation speed is over 800 rpm. However, the behavior patterns observed in the present experiment, i.e., the convex deformation at the port before the valve opens and the sudden increase in the reed displacement accompanied by the maximum bore pressure, agree with the previous experiment by the authors[15] in which a real reciprocating compressor was incorporated and operated at 1000 rpm. The basic characteristics of the opening delay are judged to be reproduced by the present experimental method.

4. 3 Comparison Between SEAT A and SEAT B

With the SEAT B, the duration of the stiction stage (Stage I) is dramatically reduced, and the opening delay is suppressed, as shown in Fig. 8(b). As a result, the maximum bore pressure with the SEAT B is 0.178 MPa, which is smaller than that of the SEAT A by about 24%. In other words, the maximum over compression difference from the discharge pressure is reduced by 43%. The maximum reed displacement at the port center is 274 μm, which is about 42% of that for the SEAT A. The bore pressure and the reed displacement settle down to 0.131 MPa and 78 μm, respectively.

Figure 14 shows the reed deformation along the *x*-axis in the stiction stage (Stage I) for both types of seats. The oil film behavior around the port with the SEAT B during the pre-rupture stage (Stage II) is shown in **Fig. 15**, and the entire area during the pre-rupture and rupture stages (Stage II and Stage III) is shown in **Fig. 16**. Figures 14 and 16 are for the test shown in Fig. 8, while the zoomed images in Fig. 15

were captured in another test. Although the same phenomena were observed with the SEAT A and SEAT B in the pre-rupture (see Fig. 15) and rupture stages (see Fig. 16), the reed deformation in the stiction stage with the SEAT B differs remarkably from that with the SEAT A (see Fig. 14). The distance between the reed and the seat at the port and its surrounding area with the SEAT B is much larger than that with the SEAT A. Particularly, the oil film thickness at the free tip end becomes much larger.

Based on the results for both the SEAT A and SEAT B, two possible factors for oil film rupture can be considered. One is the increase in the oil film thickness that accompanies the weakening of the pressure reduction in the negative squeeze oil film. In the Reynolds equation, the pressure reduction in the oil film is in inverse proportion to the third power of the oil film thickness. The larger oil film thickness with the SEAT B (see Fig. 14) easily leads to weakening of the pressure reduction in the oil film. The other factor is the pressure recovery caused by cavitation. Under a certain bore pressure, the averaged pressure in the oil film with the SEAT B must be lower than that with the SEAT A because the contact area with the SEAT B seat is smaller than that with the SEAT A. The pressure of the oil film with the SEAT B lowers easily and reaches a level under which cavitation occurs, i.e., the vapor pressure or the gas separating pressure. Both factors can explain why the oil film for the SEAT B ruptures earlier. In order to answer the question of which factor more strongly controls the oil film rupture, more case studies that vary other parameters (particularly the initial rate of the bore pressure dP_b/dt) are required.

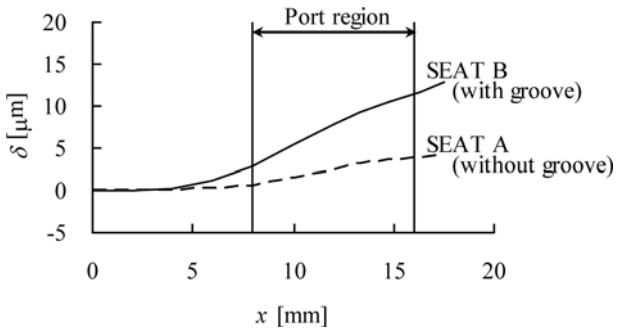

Fig. 14 Reed strain and deformation for two types of seats. (t = 7 ms in Stage I in the test shown in Fig. 8, P_b = 0.157 MPa.)

5. Summary

To understand the opening mechanism of the reed valve and the oil film on the reed/seat contact area, an experimental setup was developed to simultaneously measure reed deformation and visualize oil film behavior. Two representative valve seats with different contact areas in which a groove is added around the port of one seat were tested. As a result, the interaction of the reed deformation and the oil film behavior were clarified as follows:

(1) The opening process is divided into four stages.

Stiction stage: The reed remains stuck to the seat while the bore pressure increases. Reed deformation occurs as the bore pressure increases.

Pre-rupture stage: Cavitation occurs in the seal area around the port, and the oil film rupture starts from the tip end.

Rupture stage: The oil film ruptures, and the bore pressure starts to decrease.

Full-open stage: The reed is separated from the seat, and the gas flow settles down to a steady state.

(2) Reducing the contact area makes the duration of the stiction stage dramatically shorter and decreases

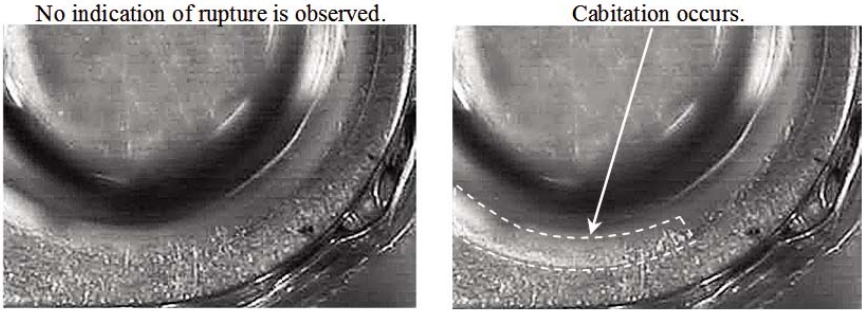

(a) $t = t_2$ - 0.1 ms (the end of Stage I) (b) $t = t_2$ + 0.3 ms (the middle of Stage II)

Fig. 15 Oil film image just before rupture. (SEAT B in Stage II; the images were captured in a test different from that of Fig. 8.)

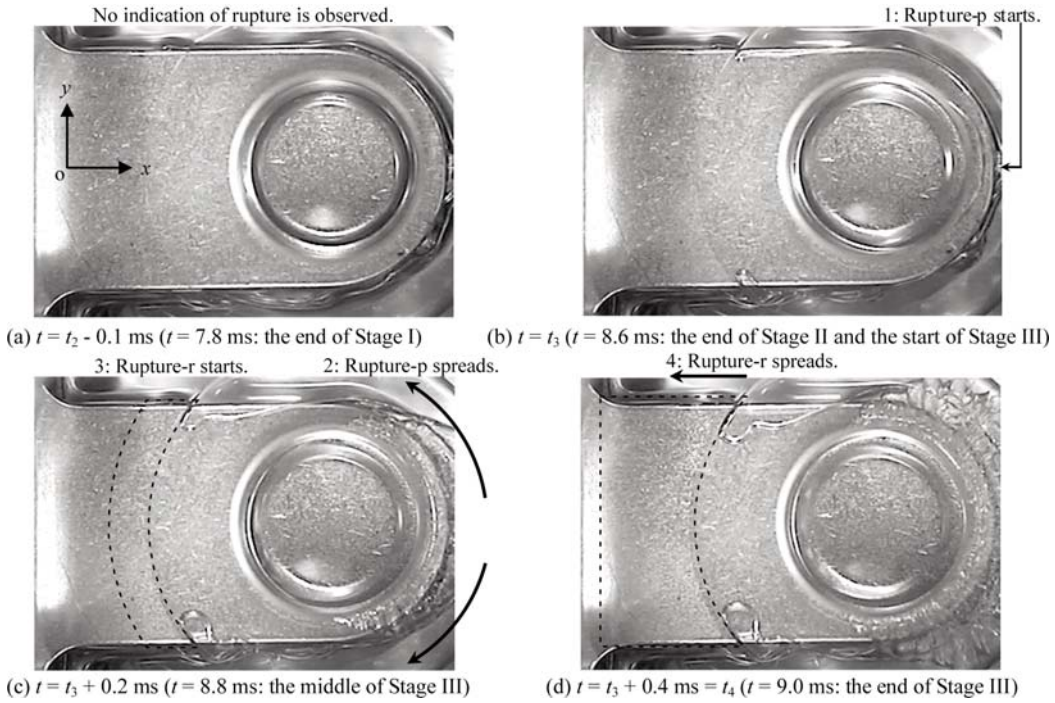

Fig. 16 Process of oil film rupture. (SEAT B in Stage II and Stage III; the images were captured in the test shown in Fig. 8.)

the opening delay. In the stiction stage, reducing the contact area has the effect of making the distance between the reed and the seat (i.e., the oil film thickness) larger, particularly at the port and its surrounding area.

(3) From the results for both types of seats with different contact areas, two possible factors in the oil film rupture can be suggested. One is the increase in the oil film thickness that accompanies weakening of the pressure reduction in the negative squeeze oil film. The other factor is the pressure recovery caused by the cavitation occurring in the oil film.

References

(1) Wambsganss, M. W. and Cohen, R., "Dynamics of a Reciprocating Compressor with Automatic Reed Valves. II, Experiments and Evaluation", *Proc. of the XII Int. Congress of Refrigeration* (1967), pp. 791-799.

(2) Brown, J. and Lough, A., "An Experimental Investigation into the Response of Disc Valves to Rapid Pressure Changes", *Proc. of the 1972 Purdue Compressor Technology Conf.* (1972), pp. 196-202.

(3) Giacomelli, E. and Giorgetti, M., "Investigation on Oil Stiction in Ring Valves", *Proc. of the 1974 Purdue Compressor Technology Conf.* (1974), pp. 167-170.

(4) Brown, J., Pringle, S., Lough, A. and Kalss, B., "Oil Stiction in Automatic Compressor Valves", *IIR Congress* (1975), pp. 1049-1059.

(5) Prasad, B. G. S. and Panayil, D., "Valve Stiction in Reciprocating Compressors", *Proc. of ASME Advanced Energy System Div.* (1996), pp. 171-180.

(6) Joo, J. M., Oh, S. K., Kim, G. K. and Kim, S. H., "Optimal Valve Design for Reciprocating Compressor", *Proc. of the 2000 Int. Compressor Eng. Conf. at Purdue* (2000), pp. 451-458.

(7) MacLaren, J. F. T. and Kerr, S. V., "Automatic Reed Valves in Hermetic Compressors", *IIR Commission III* (1969), pp. 79-86.

(8) Bauer, F., "The Influence of Liquids on Compressor Valves", *Proc. of the 1990 Int. Compressor Eng. Conf. at Purdue* (1990), pp. 647-653.

(9) Khalifa, H., E. and Liu, X., "Analysis of Stiction Effect on the Dynamics of Compressor Suction Valve", *Proc. of the 1998 Int. Compressor Eng. Conf. at Purdue* (1998), pp. 87-92.

(10) Bukac, H., "Understanding Valve Dynamics", *Sixteenth Int. Compressor Eng. Conf. at Purdue* (2002), C15-3.

(11) Courtois, S., Arnoult, E., Wagstaff, P. and Gavric, L., "On Finite Element Modeling of Valve Dynamics: Impacts, Oil Stiction, Gas Flow, …", *Sixteenth Int. Compressor Eng. Conf. at Purdue* (2002), C13-2.

(12) Yamamoto, K. and Kurosawa, J., "A Study of the Flow around the Reed Valve", *JSME Annual Meet.* (in Japanese) (2004), pp. 383-384.

(13) Yoshizumi, F., Kondoh, Y., Yoshida, K., Moroi, T., Obayashi, M., Kimura, N., Tamano, S. and Morinishi,

Y., “An Experimental Study on Opening Delay of a Reed Valve for Reciprocating Compressors”, *Proc. of ASME-JSME-KSME Joint Fluid Eng. Conf.* (2011), AJK2011-07019.
(14) Yoshizumi, F., Kondoh, Y., Yoshida, K., Moroi, T., Tamano, S. and Morinishi, Y., “Opening Delay of a Reed Valve for Refrigerant Gas Discharges in Compressors (Visualization of Oil Film Behaviors and Measurement of Valve Deformations in the Opening Process)”, *Trans. of the JSME*, *Series C* (in Japanese), Vol. 78, No. 795 (2012), pp. 3787-3802.
(15) Mizutani, T., Ito, M., Tamano, S., Kondoh, Y., Yoshida, K. and Moroi, T., ”Experimental Study on Discharge Valve Behavior and Pressure Fluctuation in a Compressor”, *Japan Soc. of Mech. Eng. Tokai Branch Conf.* (in Japanese), Vol. 58 (2009), pp.307-308.

Fumitaka Yoshizumi
Research Fields:
- Vibration Coupled with Fluid Motion
- Hydrodynamic Lubrication
- Fluid Machinery

Academic Society:
- The Japan Society of Mechanical Engineers

Kazunori Yoshida
Research Fields:
- Hydraulic/Pneumatic Equipment
- Vehicle Aerodynamics
- Textile Machinery

Academic Degree: Dr.Eng.
Academic Societies:
- The Japan Society of Mechanical Engineers
- Society of Automotive Engineers of Japan

Takahiro Moroi*
Research Fields:
- Fluid Mechanics
- Fluid Machinery
- Hydrodynamic Lubrication

Academic Degree: Dr.Eng.
Academic Societies:
- The Japan Society of Mechanical Engineers
- Society of Automotive Engineers of Japan

Award:
- Aichi invention Award, 2006 (Japan Institute of Invention and Innovation)
- The Encouragement Prize of the Chairman of Japan Patent Attorneys Association, 2006

Shinji Tamano**
Research Fields:
- Fluid Mechanics
- Non-Newtonian Fluids
- Flow Control

Academic Degree: Dr.Eng.
Academic Societies:
- The Japan Society of Mechanical Engineers
- The Japan Society of Fluid Mechanics
- The Society of Rheology
- The Society of Rheology, Japan

Award:
- JSME Young Engineers Award, 2009

Yohei Morinishi**
Research Fields:
- Fluid Mechanics
- Fluid Engineering
- Computational Fluid Dynamics
- Turbulence
- Rotating Turbulence

Academic Degree: Dr.Eng.
Academic Societies:
- The Japan Society of Mechanical Engineers
- The Japan Society of Fluid Mechanics

Awards:
- JSME Young Engineers Award, 1993
- JSFM Award for Distinguished Young Researcher in Fluid Mechanics, 1999
- JSME Tokai Branch Invention Award, 2001
- JSFM Award for Outstanding Paper in Fluid Mechanics, 2008
- JSME Fluid Engineering Division Contribution Award, 2009

*Toyota Industries Corporation
**Nagoya Institute of Technology